RF Energy Harvesting and Transfer for Spectrum Sharing Cellular IoT Communications in 5G Systems

Ali Ö. Ercan, *Senior Member, IEEE,* M. Oğuz Sunay, *Senior Member, IEEE,* and Ian F. Akyildiz, *Fellow, IEEE*

Abstract—This paper proposes an energy and spectrum efficient IoT network for 5G systems where spectrum is shared with the cellular system for spectrum efficiency and energy harvesting and energy transfer are utilized for energy efficiency. The IoT network, which consists of sensor nodes and a cluster head with a reliable energy source, reuses part of the cellular band whenever the cellular network does not utilize it. The cluster head performs spectrum sensing, random scheduling of the sensor nodes, and schedules some idle time for energy transfer. The sensor nodes harvest RF energy from the cellular traffic and the transferred energy from the cluster head. Provided the sensor nodes have sufficient energy, they transmit collected sensory data when scheduled. The inter-play between the cellular and IoT network introduces trade-offs between the spectrum availability, energy availability, information and energy transfer. This paper shows that for the same cellular traffic level, as the number of sensor nodes in the network increases, the IoT network utilization increases resulting in a multi-user gain thanks to the broadcast nature of the energy transfer. The results offer insights into different operational regimes and exposes what type of IoT applications may be feasible with such networks.

Index Terms—Cellular IoT, 5G Systems, Energy Harvesting Systems, Energy Transferring Systems

1 Introduction

In addition to the traditional human-to-human or human-to-machine communications, we are starting to increasingly observe a new trend coined as Internet of Things (IoT) [1], whereby machines around us communicate with each another with limited or no intervention from humans towards the general goal of enhanced quality of life. In this paradigm, low-cost sensors, actuators and other similar devices automatically generate, exchange and process data and act upon it towards a common goal. Many applications are envisioned, such as, healthcare [2], smart grids [3], traffic management [4], smart cities [5], agricultural systems [6], environmental monitoring [7], *etc.*

Use of cellular technologies is essential for wide area IoT systems [8]. In order to accommodate their unique challenges such as energy, spectrum, signaling overhead, upcoming 3GPP releases are targeting new enhancements for cellular IoT communications. In particular, new low-complexity, narrowband radio technologies are envisioned to support massive deployments of low throughput, low power consuming devices [9].

The motivation of this paper is to propose a unique cellular IoT system design suitable for the upcoming 5G era, where spectrum efficiency is achieved by opportunistically reusing the cellular spectrum and energy efficiency is achieved by RF energy harvesting of ambient cellular signals and RF power injection. Such a system reveals many tradeoffs between spectrum availability, energy availability, information and energy transfer. We aim to develop a through mathematical model to analyze these trade-offs, and provide the tools to be able to predict operational regimes under which such networks may be feasible.

Although wide area cellular IoT applications may deploy thousands of sensors, their aggregate traffic might not be high enough to justify allocation of dedicated cellular resources. For example, in a climate monitoring application, each sensor may generate small amounts of data over an extended period such as an hour or a day, and report all data at once. Moreover, it may be enough to query only a random fraction of these sensors and interpolate, for example the temperature/humidity values for all locations, using the collected data. Thus, this paper proposes an IoT system that reuses parts of the cellular bands in an opportunistic manner whenever the cellular devices do not utilize them [10].

Another important design constraint in massive IoT deployments is the energy. Even though individual nodes in those networks may consume little energy, their aggregate consumption may become large, necessitating a green, extremely low power design. Moreover, most of these devices are envisioned to be embedded in the environment. It is necessary to provide a way of operating them perpetually without requiring power cables or battery replacement. These requirements lead to increased interest in *energy harvesting* networks [11], [12], [13]. Various types of energy may be harvested: mechanical, electromagnetic, thermal, solar,

- *Ali. Ö Ercan and M. Oğuz Sunay are with Argela-USA, 1281 Oakmead Parkway, Suite: 201, Sunnyvale, 94085 USA.*
  E-mails: ali.ercan@argela-usa.com, oguz.sunay@argela-usa.com
- *I. F. Akyildiz is with the Broadband Wireless Networking Lab, School of Electrical and Computer Engineering, Georgia Institute of Technology, Atanta, GA 30332, USA.*
  E-mail: ian@ece.gatech.edu

This work has been partially supported by TUBITAK under Grant No. 114E739.
Manuscript received Xxx, XX, 2016; revised Xxx XX, 2017.

biological, *etc.* Among these, energy harvesting from radio frequency (RF) signals has recently attracted attention [14], [15]. Although the energy obtained from RF harvesting is currently much less compared to some other sources such as solar energy, its availability (indoors, outdoors, day or night) is advantageous. It is also expected that more efficient technologies will be developed in the near future [15], [16] to make RF energy harvesting more feasible. Thus, the proposed system in this paper consists of cellular IoT nodes that harvest RF energy from both ambient cellular signals and injected RF power to the system when the ambient RF energy is not enough.

The proposed IoT network has two types of nodes. The majority of the IoT network consists of a swarm of low cost and low power sensor nodes (SN). The other type is the cluster head (CLH), which is more powerful, control the sensor nodes and perform RF power transfer operations, as will be explained shortly. An actual IoT implementation may consist of many clusters, each with its own cluster head. This paper focuses on one such cluster.

The cellular network coexisting with the IoT network is assumed to be slotted in time and frequency. For example, LTE networks use OFDM and SC-FDM schemes in the downlink and uplink, respectively. Standardization efforts towards the 5G radio access, often referred to as 5G NX, are on-going [17]. It is foreseen that the 5G NX will be built on an enhanced, flexible OFDM-like air interface. Then, for both LTE and 5G, the radio resources are slotted in time and frequency. The resulting time-frequency slots are called cellular resource blocks. The cellular base station schedules these resource blocks to several user and control traffic data at each transmission time interval (TTI). The IoT network is assumed to operate in a time slot structure synchronous to the cellular network TTIs. Since the sensor nodes are simple and low energy, they are assumed to not use the same communication technology as the cellular network, since a requirement such as dynamically tuning to various resource blocks spanning the whole cellular band would overly increase the complexity and power consumption of SNs. Thus, in accordance with the recent IoT proposals in 3GPP [9], we assume SNs' radios are tuned to a fixed, small bandwidth, *e.g.*, spanning a few cellular resource blocks, to communicate with the cluster head using a specialized simplified physical layer for low power operation.

The proposed IoT network operation is as follows. At each TTI, the cellular network utilizes the cellular resource blocks at will regardless of the IoT network. The IoT cluster head performs spectrum sensing at the tuned bandwidth at each TTI. Whenever the cellular network is found to not use this band, the IoT network opportunistically uses it. At these opportunities, the CLH first decides to use the slot for RF energy transfer to the SNs, or for information transfer from the SNs. If the decision is information transfer, the CLH randomly schedules one SN. On the other hand if the decision is energy transfer, the CLH transmits a signal for RF energy harvesting. The SNs perform RF energy harvesting of both the ambient signals of the cellular network and injected signal by the CLH, whenever they do not perform data transmission. The interplay between sensing, energy harvesting and data/energy transmission operations, the traffic models of both cellular and IoT networks, the signaling between the CLH and SNs, retransmissions due to collisions, *etc.*, are explained in detail in Section 3.

In this work we propose for the first time, an energy and spectrum efficient IoT network for 5G, which differentiates itself from other 5G IoT proposals since spectrum sharing with the cellular network is utilized for spectrum efficiency, while energy harvesting and transmitting is utilized for energy efficiency. In this framework, we consider a system where the source of energy for sensor nodes is the RF signals in the system. We propose the use of cluster head for IoT network management as well as energy transmission when necessary. The energy harvested by the IoT devices is either from the cellular network or the cluster head. This introduces a trade-off between spectrum availability, energy availability, information and energy transfer operations: when the cellular traffic is dense, there is less spectrum opportunities but more energy from ambient harvesting, whereas a mostly idle channel presents abundant spectrum for sensor node transmission but requires more energy transfer for a feasible operation. In this paper, we also develop a thorough mathematical model to study these trade-offs where both cellular and IoT traffic are characterized more realistically compared to most work in the literature. We show that, for the same cellular traffic level, as the number of sensor nodes increases, the overall IoT network utilization increases resulting in a multi-user gain thanks to the broadcast nature of the energy transfer.

The remainder of the paper is organized as follows. We give an overview of the related work in Section 2. The system model is described in Section 3. The Markov chain modeling of the cellular and IoT traffic is given in Section 4, and the analysis based on the Markov chain models is presented in Section 5. Results are given in Section 6 and conclusions are drawn in Section 7.

2 Related Work

5G has often been labeled as the enabler of the Internet for everyone and everything. It is anticipated that by 2021 over 28 billion connected devices will exist, over 15 billion of which are forecast to be machine-to-machine connections [18]. This makes the provisioning of IoT communications one of the most important missions of 5G [19]. One fundamental aspect of IoT communications is to operate the network in a self-sufficient manner [20]. Energy harvesting is increasingly seen as a promising approach on this front [20], [21]. In this paper we propose an energy harvesting and transmitting IoT network that shares the spectrum with other services in 5G networks.

RF energy harvesting networks have been drawing significant attention in the recent literature. The works in [22], [23] assert that a practical node may either decode information or harvest RF signal energy, but not both and develop optimal switching rules for various scenarios. [24] considers a cognitive radio network where a secondary user (SU) with infinitely backlogged traffic and a simple energy consumption model performs error-free sensing, and finds the optimal allocation of time between information transfer, spectrum sensing and energy harvesting operations. [25] derives rate-energy regions for MIMO systems with three nodes: a transmitter, a decoder and an energy harvester. [16]

attempts to maximize the spatial SU throughput subject to SU transmit power and SU density in a given geography using stochastic geometry. The work assumes that an SU harvests energy from a primary user (PU) only if it is sufficiently close. [26] investigates a network where energy-harvesting SUs help increase the PU performance by relaying in return for increased spectrum access opportunities.

[27] optimizes transmission parameters of a solar energy harvesting sensor network to maximize the net throughput using Markov decision processes. [28] uses 4-D continuous-time Markov chain model for adaptive duty cycling in an energy harvesting sensor network to achieve perpetual operation with QoS provisioning. The channel model used in the paper follows a two-state Gilbert-Elliot model, akin to the busy and idle model. However, both of these works do not consider opportunistic access. The reported work in [29], [30] analyzes a system where the SUs harvest RF energy from PU signals and find optimal SU channel access policies using partially observed Markov decision processes. The incoming traffic is assumed Bernoulli. [31] considers a slotted system where each slot is divided into three durations and the SUs perform energy harvesting, spectrum sensing, and transmission exclusively. Spectrum sensing is energy detection based and done in a collaborative fashion. The optimal sensing duration, fusion rule and sensing threshold is found jointly to maximize SU throughput. No RF energy transfer is assumed in these works.

[32] considers a cognitive radio network with N SUs and M channels. Both PUs and SUs perform slotted transmission synchronously, with packets arriving according to Bernoulli processes and kept in finite queues. The PUs transmit at their dedicated channels whenever their queues are not empty. The SUs select a channel randomly, perform imperfect sensing, and transmit if the channel is found empty. The model presented in this paper has similarities to our model, however no energy harvesting, energy transmission or battery levels of the SUs are considered.

In another paper, assuming perfect channel sensing, [33] analyzes the SU queue length PMF and the packet waiting times using a 2-D continuous-time Markov chain model resulting from the assumption of decoupled SU queues. In [34], the same authors extend the analysis to general multi-interface setting and include imperfect sensing too. Both works do not consider energy harvesting or consumption.

This paper has many novelties compared to the previous literature. First, it proposes a system model for spectrum and energy efficient 5G cellular IoT network for the first time, where the spectrum efficiency is achieved by reusing part of the cellular band and the energy efficiency is achieved by harvesting of both ambient cellular RF signals and the injected RF energy. Second, the resulting tradeoffs are analyzed using a Markov Chain model that adheres to a more realistic scenario compared to the previous literature, where cellular network employs retransmissions, both networks perform queueing of incoming packets, a bursty incoming traffic is assumed as opposed to infinite back-logs, and spectrum sensing is imperfect. Third contribution of the paper is the novel application of the decoupling methodology from the 802.11 literature to the proposed 5G cellular IoT system, and investigation of its validity and limitations. As such, the modeling and analysis methodology presented in this paper can be applied to any similar system modeling.

3 System Model

The proposed cellular IoT network architecture for 5G is depicted in Figure 1, where the IoT network coexists with an OFDM or OFDM-like based cellular network such as LTE or 5G NX. The IoT network reuses a portion of the cellular band, *e.g.*, a number of contiguous resource blocks, which can be at an uplink or downlink FDD band or at a TDD band. At each transmission time interval (TTI), the cellular base station schedules user or control traffic to the resource blocks on this sub-band, without consideration of the IoT network. We assume a TTI is of duration T. For example in an LTE network, a TTI is equal to one subframe duration of 1 ms. In 5G NX, it is anticipated that the TTI value will be dynamic [17]. The proposed IoT network follows time-slotted operation synchronously with the TTI structure of the cellular network, and accesses the channel at the slots when the cellular network is found not to utilize it.

There are two types of nodes in the IoT network; a cluster head (CLH) and N_s sensor nodes (SNs). The cluster head (CLH) is powerful and connected to a reliable source of energy. An actual IoT implementation may consist of many clusters, each with its own cluster head. This paper focuses on one such cluster. At the beginning of IoT network operation, the CLH synchronizes itself to the TTI structure of the cellular network using the beacon signals transmitted by the cellular base station. During the IoT operation, the CLH is responsible to find the spectrum opportunities in the cellular sub-band, schedule the transmission of the sensor nodes at these opportunities to collect their sensory data, and perform wireless energy transfer to them. Note that the CLH is assumed to transfer the collected data to an application database either via a wired connection or over another band such as an 802.11 connection.

The sensor nodes are less powerful, but much more in numbers, running on small batteries with tight energy constraints. These nodes collect sensory data and store them in a small buffer. Whenever they are scheduled by the cluster head, they transmit for one slot duration, given they have the data and enough energy to transmit it. Otherwise, they perform energy harvesting, which is assumed to happen in two ways: from the RF energy transfer from the cluster head, which we call *RF harvesting*, or from the transmission of the cellular base station or UEs, which we call *ambient harvesting*.

The RF energy transfer is performed at the same sub-band of the cellular band that is used for IoT data transmission. When this sub-band is sensed empty, the CLH decides if it will be used for energy or data transmission. We assume that the signal characteristics of the cellular signals at this sub-band, and the signal used for RF energy transfer are similar. For example the OFDM-like signals mentioned above may also be used for RF energy transfer. As such, SNs use the same harvesting antenna and circuitry for harvesting both signals. In a practical setting, if this assumption is not valid, the IoT devices might be designed with two harvesting circuits, one for the cellular signals an the other for the RF transmission, operating in parallel. Both harvesting methods assume collection of the induced electrons at the receiving antenna of the sensor nodes in a

This article has been accepted for publication in a future issue of this journal, but has not been fully edited. Content may change prior to final publication. Citation information: DOI 10.1109/TMC.2017.2740378, IEEE Transactions on Mobile Computing

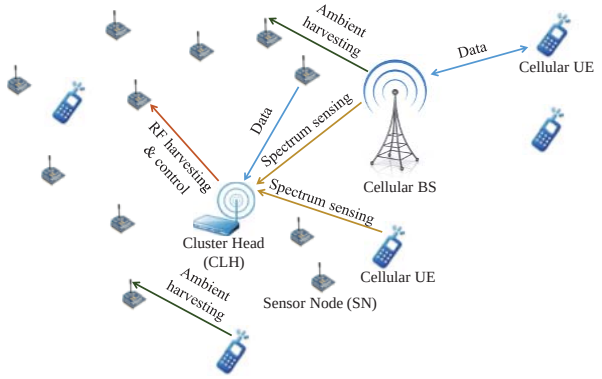

Fig. 1. Proposed spectrum sharing, energy harvesting and transmitting IoT Network.

capacitor, possibly after matching and voltage multiplying circuits [15].

The slot structure of the cellular IoT network is given in Figure 2. At the beginning of each slot, the CLH senses the channel for cellular transmission for a *sensing duration* of T_s. The actual duration of T_s depends on several factors, such as, SNR, utilized sensing method, CPU power of the CLH, *etc.*, and is out of scope of this paper. We assume that T_s is a fraction of 1 TTI. Since the paper proposes a cellular IoT system coexisting with 5G systems, as technology progresses, spectrum sensing is expected to adopt to the slot durations of 5G systems. The relation between the sensing time and missed detection / false alarm rates is discussed further in Section 4.

If the CLH decides the channel to be busy, it does nothing until the end of the slot duration. This is shown in Figure 2(a). On the other hand, if the CLH decides the channel to be free of cellular transmission, it schedules one of the SNs for transmission with probability p (Figure 2(b)), or, performs RF energy transfer to the SNs with probability $1-p$ (Figure 2(c)). If the decision is to schedule an SN, it is scheduled uniformly at random, *i.e.*, the probability that a particular SN gets scheduled given the decision to schedule an SN is $\frac{1}{N_s}$. This method is chosen over a method such as scheduling an SN with data and enough energy for transmission, in order to keep the coordination messages between the CLH and SNs unidirectional. This will further be explained below.

The scheduling decision is transmitted to the SN at a *coordination duration* of T_c. In the remaining time of the slot, namely the *utilization duration* $T_u = T - T_s - T_c$, CLH listens for scheduled SN's transmission. An SN listens to a possible scheduling message and transmits if scheduled, only when it has data and enough energy to transmit. Otherwise, an SN performs energy harvesting by default. As seen in Figure 2(a) and (b), an unscheduled SN, or a scheduled SN that does not have data or enough energy, harvests even when the CLH does not perform RF transmission, due to possible cellular network transmission. This might occur when the CLH performs a correct detection of the cellular transmission or makes a missed detection and schedules another SN.

The channel access model outlined above assumes that the coordination messages are uni-directional, from CLH to

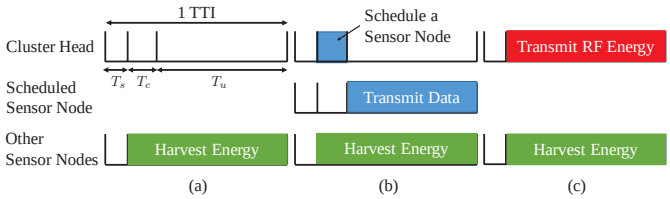

Fig. 2. Proposed slot structure of the cellular IoT network.

SNs only. This choice is made since the energy resource of SNs available for transmission is extremely scarce and it can become severely sub-optimal or even infeasible (in the energy sense) to assume that all SN nodes transmit their battery and data buffer status to the CLH periodically. However, random scheduling is sub-optimal in the achievable IoT network throughput as SNs without data or energy may be scheduled and spectrum opportunities may be missed. We demonstrate in Section 6 that this deficiency is alleviated as number of SNs increase.

The transmission of today's cellular networks utilizes hybrid ARQ mechanism, thus the cellular packets are re-transmitted up to $N-1$ times (*i.e.*, a cellular packet is transmitted up to N times) when they do not reach their destination. On the other hand, the overall application running on the IoT network is robust to packet failures. For example, a climate monitoring application usually interpolates the data collected from many sensors to construct a map of temperature, humidity, *etc.* Such operations are usually designed to utilize redundant data and tolerate missing data. Moreover, functionalities such as ARQ would increase the complexity and therefore energy expenditure of the SNs. Therefore, the SNs utilize forward error correction only, and their packets are not re-transmitted.

4 Markov Chain Modeling of Cellular and IoT Traffic

According to the model above, there is a trade-off between the time spent for transmissions and the time spent for harvesting: if more time is allocated to harvesting, there will be more energy collected to spend towards transmissions but less spectrum opportunities to do so. If more time is allocated to transmissions, there might not be enough energy. One goal of this paper is to assess this trade-off. This analysis is performed using Markov chains describing the cellular and IoT traffic models given above. In order to construct our models, we first do the following assumptions.

We assume the sensing of the channel is imperfect. The event that the CLH incorrectly decides the cellular sub-channel to be empty at a slot when the cellular network is transmitting is called a *missed detection*, and happens with probability p_{MD} independently from other slots. Similarly, the event that the CLH decides the sub-channel to be busy while it is not is called a *false alarm*, and happens with probability p_{FA} independently from other slots. In the analysis, the values of p_{MD} and p_{FA} may be chosen to match the characteristics of the sensing procedure that is used by the CLH. For example, p_{MD} and p_{FA} would be smaller when cyclostationary sensing is used, compared to energy sensing [35].

At one extreme, a sophisticated CLH may even decode the scheduling information broadcasted by the cellular BS. In this case one may assume $p_{\mathrm{MD}} = p_{\mathrm{FA}} = 0$, without losing the generality of our analysis given below. However even in this case there may be a non-zero probability of the scheduled SN not receiving the scheduling information correctly. This effectively translates into a false alarm. Moreover, if the IoT sub-band is located at an uplink FDD cellular band, the CLH may still want to reuse the channel when it is scheduled to distant cellular user equipments (UEs). In this case, a missed detection of a nearby UE may happen [36].

When a missed detection occurs and the CLH schedules an SN for transmission and the SN does so (*i.e.*, it has the data and enough energy), a collision occurs and both cellular and SN packets are assumed to be lost. The cellular packet is also lost when the CLH performs a missed detection and a subsequent RF energy transfer. As mentioned in the system model, in this case the cellular packets are assumed to be re-transmitted up to $N-1$ times. The sensor nodes on the other hand utilize forward error correction, and their packets are not re-transmitted.

We assume that aggregate cellular incoming packet traffic is generated according to an on-off process, which is widely used in the literature for bursty traffic modeling [37], [38], [39]. According to this, given no cellular packet arrived in this slot, the probability that a head-of-line packet of a burst arrives in the next slot is α. Given a packet arrived in this slot, the probability that no packet arrives in the next slot is β. The cellular packets are stored in a finite queue of size M until transmission. If a new packet arrives during the transmission of a previous packet, it is put in the queue. If the queue is full, the new packet is dropped. When the transmission of a packet is successful or maximum number of transmissions is reached, the next packet from the queue is transmitted in the next slot. Note that, since cellular transmissions are scheduled by a base station at both the uplink and the downlink, we assume an aggregate incoming traffic and a single queue for both the uplink and the downlink. Also, although we follow the previous literature to model the bursty incoming traffic via on-off Markov chain, a semi-Markov model utilizing more realistic dwelling times (compared to the geometric dwelling time of on-off Markov chain) could also be used. However, the retransmissions and queuing of the incoming packets in our model makes the transmitted traffic more realistic than the plain on-off model.

Similar to the cellular traffic, the data packet arrival process of an SN is also modeled according to an on-off process with head-of-line packet arrival probability of α_s and burst ending probability of β_s. Each SN is also assumed to utilize a finite queue of size S. As mentioned before, the SNs are assumed to use forward error correction and their packets are not retransmitted in case of a collision.

At a given slot, if the CLH finds the channel to be empty and decides to perform RF energy transmission, all SNs perform RF harvesting. RF harvesting happens even when a missed detection is made. In this case, RF energy transmission collides with cellular transmission.

In the following, all energy units are defined relative to the energy collected in one slot from ambient harvesting. We assume a total of L units of energy is collected by each SN during a slot at which RF transfer is performed. This is equivalent to assuming collected energy is L times the energy from ambient harvesting. If an SN is scheduled for transmission, has data to transmit, and has enough energy, it sends a packet. In this case we assume the SN spends K units of energy. If no RF transmission is performed and if an SN does not get scheduled or it does not have the energy or the data to transmit, then it performs ambient harvesting. If the cellular network is also simultaneously transmitting, one unit of energy is collected due to ambient harvesting. Note that even when an SN gets scheduled for transmission, if this happened after a missed detection by the CLH, another SN may still perform ambient harvesting. Total battery capacity of an SN is assumed to be B units. We assume K, L and B are integers. If all energy quantities are not integer multiples of ambient harvesting energy, one can define a smaller quantization level without losing generality of the analysis. Also, it is possible incorporate the variation of harvested energy levels due to variability of signal strengths into our analysis by defining multiple harvested energy levels. For example, given RF energy transfer is performed, an SN can be assumed to harvest energy that is equal to one of $L_1, L_2, \ldots, L_h$ units, each with an associated probability. These will introduce more branches in our Markov Chain models below. For simplicity, we assume one level of harvested energy for each type of harvesting operation.

All major parameters defined above are also listed in Table 2 in Section 6. We refer the reader to the table for a reminder of the parameters' meanings in the modeling and analysis that follow.

4.1 Decoupling Assumption

Since both networks utilize finite queues, the cellular network performs packet retransmissions and IoT network performs RF energy transfer and harvesting from the cellular traffic, the cellular and IoT networks' behaviors are highly inter-dependent. The missed detections and subsequent RF or data transmissions of the IoT network causes collisions and forces the cellular network to perform retransmissions and queueing of its incoming data. On the other hand, the ambient harvesting and spectrum opportunities available to the IoT network depend on the cellular network's transmission activity. Due to this dependence, a joint Markov chain with states representing the queue levels and the packet arrival process status of the cellular network and each sensor node, the retransmission status of the cellular network and stored energy levels of each sensor node is needed. This amounts to $O(N_s^2 MNBS)$ states, which may be prohibitively large for any numerical analysis.

In order to overcome this hurdle, we decouple the single joint Markov chain into N_s+1 separate chains, namely one cellular network and N_s sensor node (SN) chains. This way, instead of one huge chain with $O(N_s^2 MNBS)$ states, one cellular network chain with $O(MN)$ states and N_s identical SN chains with $O(BS)$ states are obtained, which need to be analyzed jointly. The details on these chains and the analysis are given in the following sections. Below, we state the underlying assumptions that we make for decoupling.

The decoupling assumption first appears in the seminal work by Bianchi [40], where several performance metrics of

a single-cell 802.11 network are analyzed using a Markov chain model of the CSMA/CA back-off window. In this work, the key (decoupling) assumption is that *the packet collision probability that all nodes experience is constant and therefore the individual back-off processes are independent*. Under this assumption, given the collision probability, an attempt probability for each node is computed, which in turn is used to compute the collision probability. This results in a fixed point equation (FPE), which is solved for the unknown collision and attempt probabilities.

The decoupling assumption and the resulting FPE method have been utilized in several following papers on the performance analysis of wireless networks, *e.g.*, [38], [41], [42]. Therefore, the validity of such an assumption has been investigated. To this end, it has been shown that a scaled version of the back-off Markov chain model converges to a non-linear ordinary differential equation (ODE) when the number of nodes in the network N grows [43]. Since the stationary point of this ODE is the same as the solution of Bianchi's FPE, the validity of the decoupling assumption turns into stability of the ODE. While it has formerly been assumed that uniqueness of the FPE solution implies validity of decoupling assumption, Cho *et al.* recently have shown that this is not always true [44]. Moreover, they have proposed a condition, which they called "Mild Intensity (MINT)," that implies the stability of the ODE. The MINT condition simply states that the attempt probability of each node at back-off stage k should scale with q_k/N, where q_k is a constant with $q_k \leq 1$ and N is the number of nodes in the network.

As detailed in Section 4.2, we decouple the cellular network Markov chain from the SN Markov chains by assuming that the collision probability ρ, that the cellular network experiences due to the transmissions of SNs, is constant. As a result of this assumption, we also solve an FPE to compute the steady-state probability mass functions (PMFs) of the decoupled Markov chains (see Section 5.2).

As explained in Section 3, a collision happens when the CLH performs a missed detection, and either performs energy transfer or schedules a sensor node with data and enough energy to transmit. For a large number of SNs, as shown by the results in Section 6, the CLH schedules an SN most of the time. Since the CLH schedules an SN uniformly at random, and since the scheduled SN might not always have data or enough energy to transmit, the attempt probability of an SN satisfies the MINT condition given above. Since our decoupling assumption is similar to the decoupling assumption in 802.11 back-off chain analysis, we conjecture that our decoupling assumption may be valid for large number of SNs and for reasonable collision probability. This is indeed observed in our results (Section 6), where the Monte-Carlo simulations of the actual model and the theoretical results using the decoupling assumption agree best when the number of SNs is large and probability of missed detection p_{MD} is low. On the other hand the deviation becomes larger as the number of SNs gets smaller or as p_{MD} gets larger.

4.2 Cellular Network Markov Chain Model

The Markov chain model for the cellular network operation is given in Figure 3. The states of the cellular network chain are three dimensional. State (i, j, k) denotes that there are i packets in the cellular network queue ($i \in \{0, 1, \dots M\}$), the current packet is transmitted for the j^{th} time ($j \in \{0, 1, \dots N\}$, $j = 0$ means there is no transmission), and $k \in \{0, 1\}$ denotes the status of the packet arrival process. $k = 0$ means the packet in the next slot, if arrives, is a continuation packet of an ongoing burst; where as $k = 1$ means it is the first packet of a new burst.

The variable ρ that appears in the transition probabilities of the cellular network Markov chain is the probability of packet collision, given an ongoing cellular transmission. With the decoupling assumption, we assume ρ is a constant function of the SN chain PMF. The computation of ρ requires solving the cellular and SN chains' PMFs jointly, which is explained in Section 5.2.

All the transitions *from* the states $(0, 0, 1)$, $(0, j, 1)$ (valid for $1 \leq j < N$), $(0, N, 1)$, $(i, j, 0)$, $(i, j, 1)$ (valid for $1 \leq i < M$ and $1 \leq j < N$), $(i, N, 0)$, $(i, N, 1)$ (valid for $1 \leq i < M$), $(M, j, 0)$, $(M, j, 1)$ (valid for $1 \leq j < N$), $(M, N, 0)$ and $(M, N, 1)$ are given in Figure 3. With the said ranges for i and j, these represent all states including the corner cases. The states from which the transitions originate are shaded in the figure to distinguish them from the destination states.

The state $(0, 0, 1)$ is the idle state, since the queue is empty and there is no cellular transmission. The next packet is head-of-line, and if it arrives (with probability α), the state moves to $(0, 1, 0)$ since the following packet will be a continuation packet. At state (i, j, k), if a collision occurs, the state moves to the next column since the cellular packet is retransmitted. If a new packet arrives at the same time, the queue is incremented and the following packet will be a continuation packet, so the state moves to $(i+1, j+1, 0)$. The probability of this event is $\alpha\rho$ if $k = 1$ and $(1-\beta)\rho$ if $k = 0$. If a collision occurs but a new packet does not arrive, the next packet will be head-of-line, so the state moves to $(i, j+1, 1)$. The probability of this event is $(1 - \alpha)\rho$ if $k = 1$ and $\beta\rho$ if $k = 0$. If the packet is sent successfully, the state moves to the first column since the next packet will be transmitted for the first time. If no new packet arrives, and there are no packets in the queue, the state moves to idle state $(0, 0, 1)$. If no new packet arrives but there is at least one packet in the queue, the queue is decremented, the packet from the queue is transmitted for the first time, and the following packet will be head-of-line, so state moves to $(i - 1, 1, 1)$. The probabilities for both events are $(1 - \alpha)(1 - \rho)$ if $k = 1$ and $\beta(1 - \rho)$ if $k = 0$. If a new packet arrives, the queue stays the same, and the next packet will be continuation, so the state moves to $(i, 1, 0)$. The probability of this event is $\alpha(1 - \rho)$ if $k = 1$ and $(1 - \beta)(1 - \rho)$ if $k = 0$.

Note that in the first row, the states $(0, j, 0)$ do not exist for $j > 1$ since here, the queue is empty and cellular network is retransmitting, thus any new packet must be head-of-line. On the other hand, the state $(M, 1, 1)$ does not exist in the last row since $(i, 1, 1)$ nodes have incoming transitions only from the nodes in the row below. Thus, there are a total of $2MN + N + 1$ states.

4.3 Sensor Node Markov Chain Model

The Markov Chain model for the operation of an SN is given in Figure 4. Given the random scheduling scheme of

This article has been accepted for publication in a future issue of this journal, but has not been fully edited. Content may change prior to final publication. Citation information: DOI 10.1109/TMC.2017.2740378, IEEE Transactions on Mobile Computing

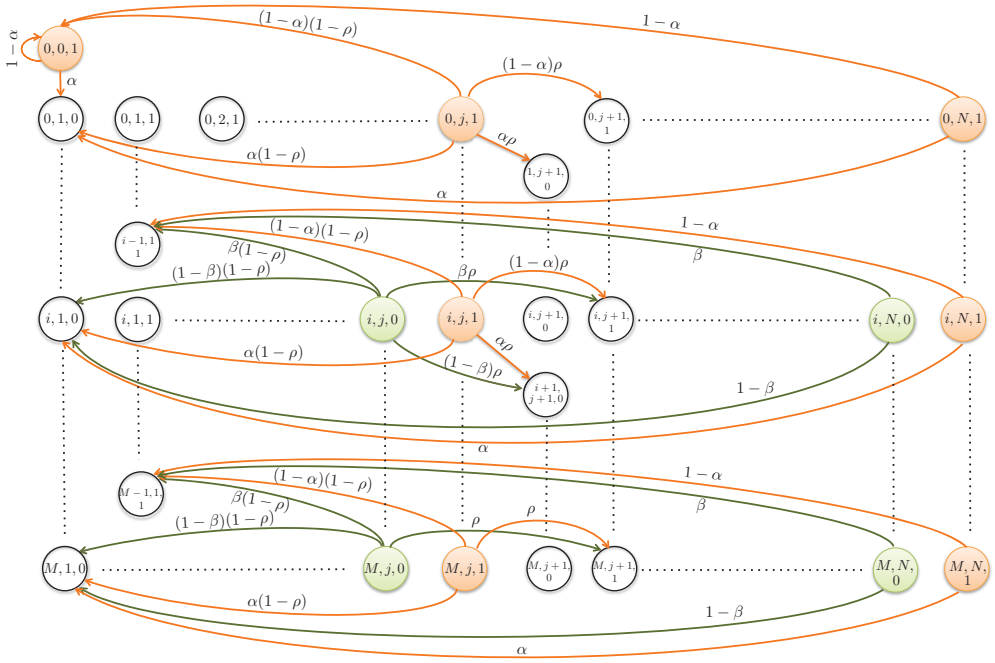

Fig. 3. Cellular network Markov chain. State (i, j, k) denotes there are i packets in the cellular network queue, the current packet is transmitted for the j^{th} time, and k denotes the status of the packet arrival process. $k = 0$ means the packet in the next slot, if arrives, is a continuation packet of an ongoing burst; whereas $k = 1$ means it is the first packet of a new burst. ρ denotes the probability of packet collision, given an ongoing cellular transmission.

the SNs and the decoupling assumption, there are a total of N_s identical and independent Markov chains as in Figure 4 running in parallel, each modeling the behavior of one SN. In the figure, state (i, j, k) denotes there are i packets in the queue ($i \in \{0, 1, \dots S\}$), the battery level is $B - j$, ($j \in \{0, 1, \dots B\}$ and $j = 0$ means a full battery), and $k \in \{0, 1\}$ denotes the status of the packet arrival process, which is defined in the same manner to the cellular network chain.

In Figure 4, p_1 through p_5 are probabilities that are defined below. These are functions of the cellular network chain, and with the decoupling assumption they are assumed constant.

$$p_1 = \mathbb{P}(\text{SN is not scheduled for transmission and does not perform energy harvesting.}) \quad (1)$$

$$p_2 = \mathbb{P}(\text{SN is not scheduled for transmission and performs ambient harvesting.}) \quad (2)$$

$$p_3 = \mathbb{P}(\text{SN is not scheduled for transmission and performs RF harvesting.}) \quad (3)$$

$$p_4 = \mathbb{P}(\text{SN is scheduled for TX, doesn't have the energy, does not perform harvesting.}) \quad (4)$$

$$p_5 = \mathbb{P}(\text{SN is scheduled for TX, doesn't have the energy, performs ambient harvesting.}) \quad (5)$$

It is shown in the Appendix that these probabilities are given by

$$p_1 = \pi_0 \left(p_{\text{FA}} + (1 - p_{\text{FA}}) p \frac{N_s - 1}{N_s} \right), \quad (6)$$

$$p_2 = (1 - \pi_0) \left(1 - p_{\text{MD}} + p_{\text{MD}} p \frac{N_s - 1}{N_s} \right), \quad (7)$$

$$p_3 = (1 - p) \left((1 - \pi_0) p_{\text{MD}} + \pi_0 (1 - p_{\text{FA}}) \right), \quad (8)$$

$$p_4 = \pi_0 (1 - p_{\text{FA}}) \frac{p}{N_s}, \quad (9)$$

$$p_5 = (1 - \pi_0) p_{\text{MD}} \frac{p}{N_s}, \quad (10)$$

where π_0 is the steady-state probability of the channel being free of cellular transmission, which is equal to the steady-state probability of the cellular network chain state (0,0,1). The computation of π_0 requires solving the cellular network and SN PMFs jointly. This is explained in Section 5.2. Note that, in addition to the events defined above, the probability of an SN getting scheduled is $p_4 + p_5$, since the CLH schedules a sensor if the channel is empty and no missed detection is performed, or is not empty and a false alarm happens, and no energy transfer is performed.

The transitions from the states that are representative of all cases are given in Figure 4. In the first and the second rows, the SN has enough energy for one transmission, whereas, it cannot transmit due to insufficient energy in the last row. The states $(i, 0, 0)$ and $(i, 0, 1)$ in the first row represent all states with $0 < i < S$; the states $(0, j, 0)$ and $(0, j, 1)$ in the second row represent all states with $0 < j \leq B - K$; the states $(i, j, 0)$ and $(i, j, 1)$ in the second row represent all states with $0 < i < S$ and $0 < j \leq B - K$, and the states $(i, j, 0)$ and $(i, j, 1)$ in the third row represent all states with $0 \leq i < S$ and $B - K < j \leq B$. There are a total of $2BS + 2(B + S) + 1$ states.

For example, let us examine the (i, j, k) states in the second and third rows. At the the second row, the SN has enough energy for transmission. Thus, if no packet arrives, SN is not scheduled and no harvesting occurs (there is no

This article has been accepted for publication in a future issue of this journal, but has not been fully edited. Content may change prior to final publication. Citation information: DOI 10.1109/TMC.2017.2740378, IEEE Transactions on Mobile Computing

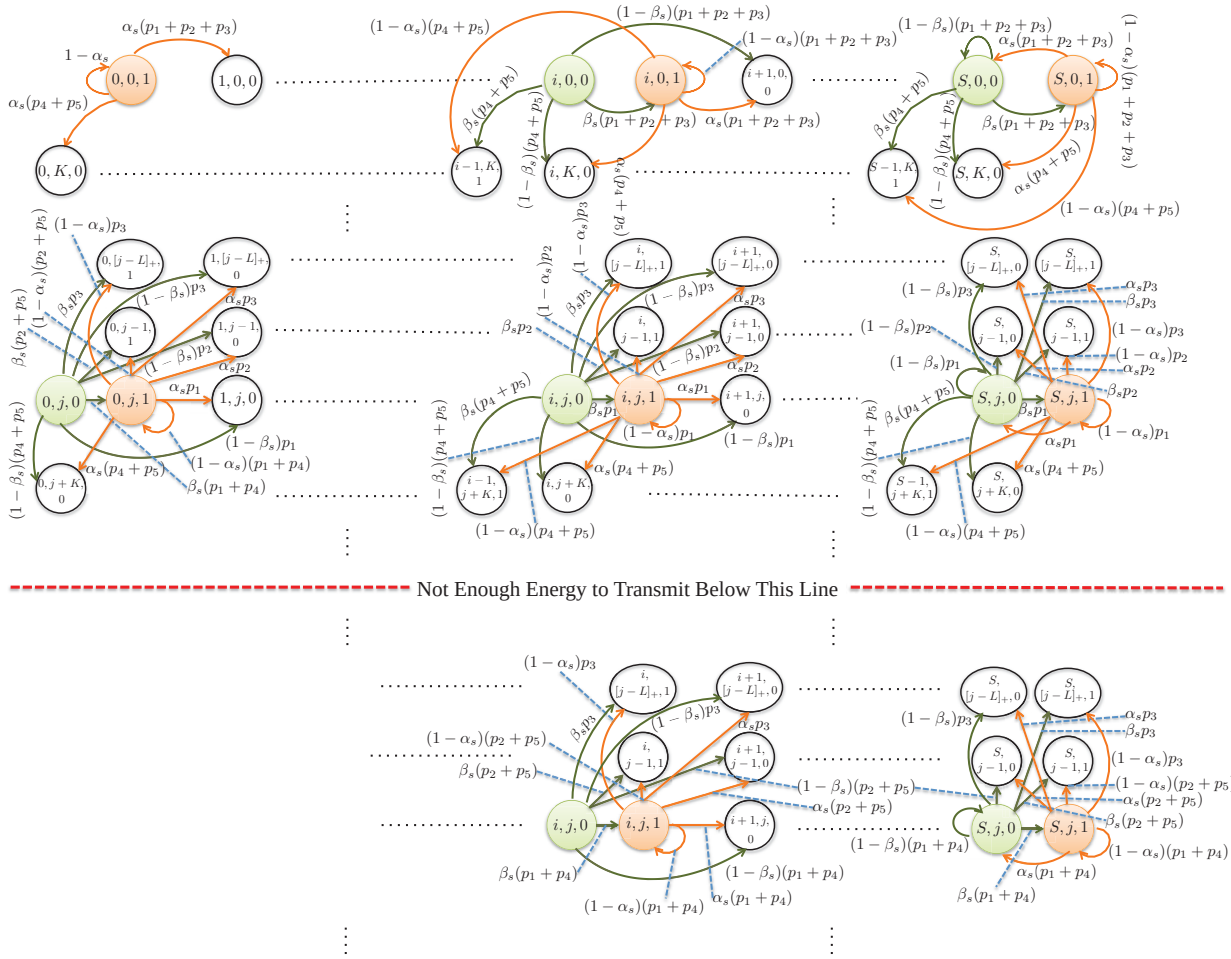

Fig. 4. SN Markov chain. State (i, j, k) means there are i packets in the queue, battery level is $B - j$.$k = 0$ means the packet in the next slot, if arrives, is a continuation packet of an ongoing burst; where $k = 1$ means it is the first packet of a new burst.

ongoing cellular transmission), the next packet will be head-of-line, so the state moves to $(i, j, 1)$. The probability of this event according to the definitions above is $(1 - \alpha_s)p_1$ if $k = 1$ and $\beta_s p_1$ if $k = 0$. If no packet arrives, SN is not scheduled, and ambient harvesting occurs, battery charges by one unit and the state moves to $(i, j - 1, 1)$. The probability of this event is $(1 - \alpha_s)p_2$ if $k = 1$ and $\beta_s p_2$ if $k = 0$. If no packet arrives, SN is not scheduled, and RF energy transfer harvesting occurs, battery charges by L units the state moves to $(i, [j - L]_+, 1)$. Here $[x]_+ := \max\{0, x\}$ since when the battery becomes full, it stops charging. The probability of this event is $(1 - \alpha_s)p_3$ if $k = 1$ and $\beta_s p_3$ if $k = 0$. If no packet arrives and SN is scheduled, it transmits one packet from the queue and the battery drains by K units so the state moves to $(i - 1, j + K, 0)$. The probability of this event is $(1 - \alpha_s)(p_4 + p_5)$ if $k = 1$ and $\beta_s(p_4 + p_5)$ if $k = 0$. When there is not enough energy for transmission (third row of states in the figure), the SN always performs harvesting whether or not it is scheduled. So, if a new packet arrives and no harvesting occurs, the queue increases by one, the state moves from (i, j, k) to $(i + 1, j, 0)$, with probability $\alpha_s(p_1 + p_4)$ if $k = 1$ and $(1 - \beta_s)(p_1 + p_4)$ if $k = 0$. A comprehensive list of all possible events, the corresponding state transitions and associated probabilities

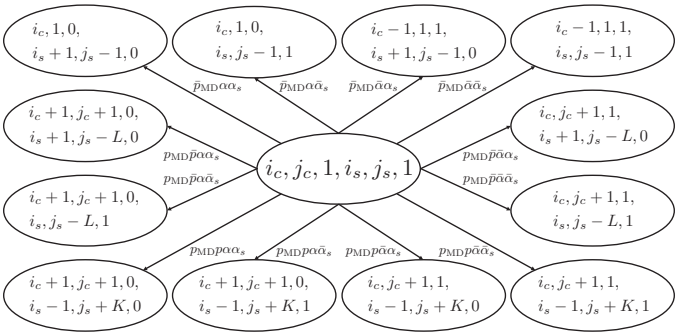

Fig. 5. Transitions from joint Markov chain state $(i_c, j_c, 1, i_s, j_s, 1)$. It is assumed there is one SN, both cellular and SN queues are neither empty nor full ($0 < i_c < M$, $0 < i_s < S$), the SN has enough energy to transmit and its battery is at least L units depleted ($L \leq j_s \leq B - K$), and the cellular network is currently transmitting but has not reached maximum number of transmissions ($0 < j_c < N$). For brevity, $\bar{x}$ is used instead of $1 - x$ in the transition probabilities.

are given in Table 1.

4.4 An Example Case of a Joint Markov Chain

In order to compare the decoupled Markov chains to the joint Markov chain, as an example, the transitions and

This article has been accepted for publication in a future issue of this journal, but has not been fully edited. Content may change prior to final publication. Citation information: DOI 10.1109/TMC.2017.2740378, IEEE Transactions on Mobile Computing

TABLE 1
The SN Markov chain transitions. Below, use $\gamma_s = \alpha_s$ when $k = 1$, and $\gamma_s = 1 - \beta_s$ when $k = 0$.

Origin st.	Enough TX energy?	Sched?	Harvesting?	New pack. arrives?	Next state	Probability
(i, j, k)	✔	✔	–	✔	$(i, j + K, 0)$	$\gamma_s(p_4 + p_5)$
(i, j, k)	✔	✔	–	✖	$(i - 1, j + K, 1)$	$(1 - \gamma_s)(p_4 + p_5)$
(i, j, k)	✔	✖	No	✔	$(i + 1, j, 0)$	$\gamma_s p_1$
(i, j, k)	✔	✖	Ambient	✔	$(i + 1, j - 1, 0)$	$\gamma_s p_2$
(i, j, k)	✔	✖	RF	✔	$(i + 1, [j - L]_+, 0)$	$\gamma_s p_3$
(i, j, k)	✔	✖	No	✖	$(i, j, 1)$	$(1 - \gamma_s)p_1$
(i, j, k)	✔	✖	Ambient	✖	$(i, j - 1, 1)$	$(1 - \gamma_s)p_2$
(i, j, k)	✔	✖	RF	✖	$(i, [j - L]_+, 1)$	$(1 - \gamma_s)p_3$
(i, j, k)	✖	–	No	✔	$(i + 1, j, 0)$	$\gamma_s(p_1 + p_4)$
(i, j, k)	✖	–	Ambient	✔	$(i + 1, j - 1, 0)$	$\gamma_s(p_2 + p_5)$
(i, j, k)	✖	–	RF	✔	$(i + 1, [j - L]_+, 0)$	$\gamma_s p_3$
(i, j, k)	✖	–	No	✖	$(i, j, 1)$	$(1 - \gamma_s)(p_1 + p_4)$
(i, j, k)	✖	–	Ambient	✖	$(i, j - 1, 1)$	$(1 - \gamma_s)(p_2 + p_5)$
(i, j, k)	✖	–	RF	✖	$(i, [j - L]_+, 1)$	$(1 - \gamma_s)p_3$

corresponding transition probabilities from the joint state $(i_c, j_c, 1, i_s, j_s, 1)$ is given in Figure 5. For the sake of illustration, only one SN is assumed to exist in the IoT network, since assuming more SNs would result in a prohibitively large state and complex transitions. Here, similar to the decoupled chains, i_c and i_s denote the number of packets in the cellular and SN queues, respectively, j_c denotes the transmission attempt number for the currently transmitted cellular packet, j_s denotes the battery level of the SN. 1's denote the packet arrival process status; meaning for this state, next arriving packet is head-of-line for both the cellular network and the SN. Here, it is assumed that both cellular and SN queues are neither empty nor full ($0 < i_c < M$, $0 < i_s < S$), the SN has enough energy to transmit and its battery is at least L units depleted ($L \leq j_s \leq B - K$), and the cellular network is currently transmitting but has not reached maximum number of transmissions ($0 < j_c < N$).

The transitions to the top row of states correspond to the cases when the CLH does a correct detection of the cellular transmission, and therefore the SN performs ambient harvesting and cellular transmission is successful. The transitions to the bottom row of states correspond to the cases when the CLH makes a missed detection, and schedules the SN for transmission. Since the SN has at least a packet in its queue and has enough energy, it attempts transmission and collision occurs. The transitions to the states in the middle left and right correspond to the cases when the CLH performs a missed detection and energy transfer. Again the cellular transmission is not successful but the SN performs RF harvesting.

In the transition probabilities, $\bar{x}$ is used instead of x for brevity. All transition probabilities in the joint Markov chain are constant and thus, no need for the assumptions in decoupling. However, even when there is only one SN, the joint MC state is large, resulting in many different cases. Note that, Figure 5 depicts only one specific case. For a practical IoT system with many nodes, the joint chain would be prohibitively complex for any analysis, which illustrates the necessity of decoupling assumption.

5 Analysis

We define the channel utilization levels of the cellular or IoT networks as the long term averages of the ratios of slots with successful packet transmissions to total number of slots. By this definition, we do not discount for the time that the IoT network loses for sensing and coordination. However, one may alternatively scale IoT utilization appropriately.

In this section, the channel utilization levels of the cellular and IoT networks are derived. First, an approximate analysis that does many simplifying assumptions will be presented to provide a baseline understanding of the trade-offs in the operation of a cellular IoT network employing opportunistic spectrum access, RF energy transfer and harvesting. Then a more realistic analysis that uses the Markov chain models given above will be presented in Section 5.2.

5.1 Simple Approximation

It is possible to calculate cellular and IoT utilization levels easily for a simplified system model. Assume a system where all SNs are infinitely backlogged. Furthermore, assume that the cellular network retransmits collided packets until they are successfully transmitted. This is equivalent to assuming that the cellular network has an infinite queue and the maximum number of cellular retransmissions goes to infinity. In the absence of any collisions, the cellular utilization due to the incoming traffic is

$$Q_C = \frac{\alpha}{\alpha + \beta}. \tag{11}$$

Assuming that the SNs are infinitely backlogged and they have enough transmission energy, a collision occurs each time the CLH performs a missed detection. Thus, accounting for the collisions, the portion of the channel that is occupied by the cellular network should be equal to

$$C_C = Q_C \sum_{n=0}^{\infty} (p_{\mathrm{MD}})^n = \frac{\alpha}{\alpha + \beta} \frac{1}{1 - p_{\mathrm{MD}}}, \tag{12}$$

This article has been accepted for publication in a future issue of this journal, but has not been fully edited. Content may change prior to final publication. Citation information: DOI 10.1109/TMC.2017.2740378, IEEE Transactions on Mobile Computing

since retransmissions occur every time there is a collision. The portion of the channel where collisions are experienced is then equal to

$$C_X = C_C - Q_C = \frac{\alpha}{\alpha+\beta}\frac{p_{\rm MD}}{1-p_{\rm MD}}. \quad (13)$$

Note that, since the CLH performs RF energy transmission with probability $(1-p)$ when it detects the channel to be empty, a fraction of $(1-p)C_X$ of these collisions are due to CLH RF energy transfer and a fraction of pC_X of these collisions are due to SN transmissions. The channel remains idle when the cellular network does not transmit and the CLH performs a false alarm. Then, the portion of the channel that is idle is equal to

$$C_I = (1-C_C)p_{\rm FA}. \quad (14)$$

In addition to the $(1-p)C_X$ term above, CLH performs RF energy transfer with probability $(1-p)$ whenever the channel is empty and the CLH does not perform a false alarm. Thus, the total portion of the channel occupied by the CLH for RF energy transfer is equal to

$$C_{RF} = \underbrace{(1-C_C)\,(1-p_{\rm FA})(1-p)}_{\text{channel empty}} + \underbrace{(1-p)\,C_X}_{\text{collisions}}. \quad (15)$$

SNs also perform ambient harvesting at the portion of the channel utilized by the cellular network and not collided with the CLH, thus, ambient harvesting is performed in the $C_C-(1-p)C_X$ portion of the channel. Since for a unit time, the energy harvested from RF transfer is L times, and the energy spent for transmission is K times the energy gained from ambient harvesting, respectively, we get an energy limit on the portion of the channel that may be utilized by SN transmissions as

$$U_S^e = \frac{LC_{RF} + C_C - (1-p)C_X}{K}. \quad (16)$$

On the other hand, the spectrum availability gives the other limit. That is, an SN may utilize a fraction $\frac{1}{N_s}$ of the portion of the channel that is sensed correctly to be free and scheduled for SN transmission

$$U_S^s = \frac{(1-C_C)(1-p_{\rm FA})p}{N_s}. \quad (17)$$

Minimum of these two limits give the overall portion of the channel utilized by one SN for transmissions. Since there are N_s SNs, the portion of the channel utilized by all N_s SNs is equal to,

$$U_S^{\rm approx} = N_s \min\left\{U_S^e, U_S^s\right\}, \quad (18)$$

which is an approximation to the IoT network utilization level.

We observed in the simulations that as there are more SNs ($N_s \to \infty$) and as the SN data generation becomes more bursty ($\beta_s \to 1$), this simplified approximation becomes more realistic. However it is quite far from being realistic when these are not the case, as shown in the Results (Section 6). Next, we present the analysis of the full model where SN traffic is not infinitely backlogged but bursty, and the cellular network has a finite queue size and performs a finite maximum number of retransmissions for collided packets.

5.2 Markov Chain Analysis

Given the decoupling assumption, the cellular and SN Markov chains are finite-state, irreducible, and aperiodic, implying that all states are positive recurrent and ergodic. Thus, there exist unique steady-state PMFs of the states of these Markov chains [45]. The cellular or SN utilizations are defined as the long-term averages of the ratios of slots with successful packet transmissions to total number of slots. Due to ergodicity, this is equal to the probability that a slot is used for a successful transmission of a packet. Since the short-term transients get averaged out in the long-term, the steady-state PMFs of the Markov chains are used to compute the probabilities to find the utilization levels. The steady-state PMFs are calculated as follows.

First, define $\Pi^{\rm C}_{i,j,k}$ as the steady-state probability of the cellular network chain to be in the state (i,j,k). Since N_s SN Markov chains are identical, all of their steady-state PMFs are the same. Thus, define $\Pi^{\rm SN}_{i,j,k}$ as the probability of any SN chain to be in the state (i,j,k) in steady state.

Define one-to-one mappings $\ell_C : \mathbb{Z}_+^3 \to \mathbb{Z}_+$ and $\ell_S : \mathbb{Z}_+^3 \to \mathbb{Z}_+$ that map the three dimensional indices of the cellular and SN Markov chain states, respectively, to one dimensional indices. Here, $\mathbb{Z}_+$ denotes the set of non-negative integers. Then, given ρ, which is the probability of packet collision with an SN given an ongoing cellular transmission, the steady state PMF of cellular network Markov chain can be found as the unique Perron-Frobenius left eigenvector of the state transition matrix $P^{\rm C}(\rho)$,

$$\boldsymbol{\pi}_{\rm C}^T P^{\rm C}(\rho) = \boldsymbol{\pi}_{\rm C}^T, \quad (19)$$

where

$$m := \ell_C(i',j',k'),\ n := \ell_C(i,j,k) \quad (20)$$

$$[P^{\rm C}(\rho)]_{n,m} := \mathbb{P}(X^{\rm C}(t+1) = (i',j',k') | X^{\rm C}(t) = (i,j,k)). \quad (21)$$

Above, $X^{\rm C}(t)$ denotes the cellular network Markov chain, t denotes time index, the transition probabilities in Equation (21) are specified in Figure 3, and $\boldsymbol{\pi}_{\rm C}$ is assumed to be normalized such that its elements sum to one. Then $\Pi^{\rm C}_{i,j,k}$ are simply elements of $\boldsymbol{\pi}_{\rm C}$, *i.e.*, $\Pi^{\rm C}_{i,j,k} = \boldsymbol{\pi}_{\rm C}[n]$.

Similarly, given π_0, which is simply equal to $\Pi^{\rm C}_{0,0,1}$, and the decoupling assumption, the steady state PMF of SN Markov chain can be found as follows

$$\boldsymbol{\pi}_{\rm SN}^T P^{\rm SN}(\pi_0) = \boldsymbol{\pi}_{\rm SN}^T, \quad (22)$$

where

$$m := \ell_S(i',j',k'),\ n := \ell_S(i,j,k) \quad (23)$$

$$[P^{\rm SN}(\pi_0)]_{n,m} := \mathbb{P}(X^{\rm SN}(t+1) = (i',j',k') | X^{\rm SN}(t) = (i,j,k)). \quad (24)$$

Above, $X^{\rm SN}(t)$ denotes the SN Markov chain, the transition probabilities are given in Figure 4 and in Table 1, and $\boldsymbol{\pi}_{\rm SN}$ is assumed to be normalized such that its elements sum to one. Then $\Pi^{\rm SN}_{i,j,k}$ are simply elements of $\boldsymbol{\pi}_{\rm SN}$, *i.e.*, $\Pi^{\rm SN}_{i,j,k} = \boldsymbol{\pi}_{\rm SN}[n]$.

The parameter ρ is the probability of collision given the cellular network is transmitting, which happens if the CLH performs a missed detection, and then either decides to do

an RF energy transfer or schedules an SN that has a packet to send and enough energy to do so, which in turn happens if the SN has enough energy ($j \leq B-K$) and if it has at least one packet in its queue ($i \geq 1$) or a new packet arrives. Thus ρ is given by

$$\rho = p_{\text{MD}} \left[(1-p) + p \left((1-\beta_s) \sum_{j=1}^{B-K} \Pi^{\text{SN}}_{0,j,0} + \alpha_s \sum_{j=0}^{B-K} \Pi^{\text{SN}}_{0,j,1} + \sum_{i=1}^{S} \sum_{j=0}^{B-K} \sum_{k=0}^{1} \Pi^{\text{SN}}_{i,j,k} \right) \right]. \quad (25)$$

We numerically solve the equations (19), (22) and (25) jointly to compute the cellular and SN Markov chain PMFs, as well as the parameters $\pi_0 = \Pi^{\text{C}}_{0,0,1}$ and ρ. Then these PMFs are used to compute the utilization levels as follows.

5.2.1 Cellular Network Utilization

Note that a cellular packet is not transmitted if one of the following mutually exclusive events happen.

i) *Queue Overflow* (QO): Cellular queue is full, a new packet arrives, the current transmission collides with an SN, maximum number of cellular transmissions have not been reached.
ii) *Maximum Retransmissions* (MR): A collision happens after maximum number of cellular retransmissions is reached.

Thus, the probability of a cellular packet to be successfully transmitted (ST) is

$$\mathbb{P}(\text{ST}) = 1 - \mathbb{P}(\text{QO}) - \mathbb{P}(\text{MR}). \quad (26)$$

Given the steady-state PMF of the cellular network Markov chain, the probabilities above are given by

$$\mathbb{P}(\text{QO}) = (1-\beta)\rho \sum_{j=1}^{N-1} \Pi^{\text{C}}_{M,j,0} + \alpha\rho \sum_{j=2}^{N-1} \Pi^{\text{C}}_{M,j,1}, \quad (27)$$

$$\mathbb{P}(\text{MR}) = \rho \sum_{i=1}^{M} \Pi^{\text{C}}_{i,N,0} + \rho \sum_{i=0}^{M} \Pi^{\text{C}}_{i,N,1}. \quad (28)$$

The cellular channel utilization is then the cellular utilization in the absence of opportunistic IoT network access, times the success probability,

$$U_C = \frac{\alpha}{\alpha+\beta} \mathbb{P}(\text{ST}). \quad (29)$$

5.2.2 IoT Network Utilization

An SN performs a successful transmission at a slot if one of the following mutually exclusive events happen:

i) ST1: Cellular network is not transmitting, CLH does not make a false alarm, SN is scheduled for transmission, it has enough energy to transmit, SN queue is empty but a new packet arrives.
ii) ST2: Cellular network is not transmitting, CLH does not make a false alarm, SN is scheduled for transmission, it has enough energy to transmit, SN queue is not empty.

The probabilities of these events are given by

$$\mathbb{P}(\text{ST1}) := \pi_0(1-p_{\text{FA}}) \frac{p}{N_s} \left[(1-\beta_s) \sum_{j=1}^{B-K} \Pi^{\text{SN}}_{0,j,0} + \alpha_s \sum_{j=0}^{B-K} \Pi^{\text{SN}}_{0,j,1} \right] \quad (30)$$

$$\mathbb{P}(\text{ST2}) := \pi_0(1-p_{\text{FA}}) \frac{p}{N_s} \sum_{i=1}^{S} \sum_{j=0}^{B-K} \sum_{k=0}^{1} \Pi^{\text{SN}}_{i,j,k}. \quad (31)$$

Thus, for N_s SNs, the IoT network utilization is given by

$$U_S = N_s \frac{\alpha_s}{\alpha_s+\beta_s} (\mathbb{P}(\text{ST1}) + \mathbb{P}(\text{ST2})). \quad (32)$$

6 Results

In this section we present results obtained through our detailed Markov chain model for different system parameters, comparing them with Monte Carlo simulations. In the experiments, the system parameters used by default, unless otherwise stated, are given in Table 2. The Monte Carlo simulations have been conducted for 1,000,000 time slots and repeated 25 times. The simulations are time-driven. N_s+1 packet arrival processes, one for the cellular network and N_s processes for the SNs are simulated. Each slot, when the cellular network has packets in its queue or when the queue is empty but a new packet arrives, it attempts to send a packet. If the packet collides with any SN transmission, then it is retransmitted in the next slot. A maximum of N transmission attempts are done for a packet. The arriving packets during transmissions are placed in the queue. If the queue is full, the incoming packets are dropped.

For each run, the initial battery levels of the individual SNs are assumed to be i.i.d. and uniform over $[0, B]$. The incoming packets of an SN are also put in a queue to be sent when the SN is scheduled and has enough energy for transmission. The SNs don't retransmit collided packets. The incoming packets are dropped when their queues are full. According to the nature of the IoT application, one may alternatively think that the oldest packet is dropped to make room for a new packet, when the SN queue is full. This makes no difference on the following results. The sensing, scheduling, RF energy transfer, energy harvesting and data transmission operations are performed by the CLH and SNs as explained in Section 3. For a given run, the cellular or IoT utilization levels are calculated as the ratio of the number of slots resulted in successful transmissions to the total number of slots. The average utilizations over 25 Monte-Carlo runs are reported in the figures. For the IoT network, sum utilization levels of all SNs are reported. The standard deviations observed for each simulated utilization level are found to be much smaller than the corresponding mean values. We demonstrate in the results presented below that the Markov chain analysis closely follows the Monte-Carlo simulations especially for large number of sensor nodes and small missed detection probability, as explained in Section 4.1.

First, we investigate the IoT network utilization as a function of the SN scheduling probability, p. This is illustrated in Figure 6 for 1, 50 and 500 sensor nodes present in

TABLE 2
Default parameters used in the simulations, unless specified otherwise.

Param.	Description	Default
α	Cellular head-of-line packet probability	0.5
β	Cellular burst ending probability	0.5
M	Cellular queue size	10
N	Max number of tx. of a cellular packet	7
p_{MD}	Prob. of CLH performing a missed detection	0.05
p_{FA}	Probability of CLH performing a false alarm	0.05
p	Prob. sched. SN, given channel found empty	0.5
α_s	SN head-of-line packet probability	0.01
β_s	SN burst ending probability	0.99
B	SN battery capacity	110
S	SN queue size	3
K	Energy consumed by SN to txmit one packet	100
L	Energy gained by RF energy transfer	1

the network. We observe that there is an optimal scheduling probability p^*, in each case. For values of $p < p^*$, the performance of the IoT network is limited by insufficient available spectrum, as the portion of the channel not occupied by the cellular network is largely used for energy transfer for these p values. When $p > p^*$ on the other hand, the IoT utilization becomes bounded by available energy at the sensor nodes. As p increases, energy transfer becomes less frequent, and as a consequence the SN utilizations decrease. For large number of sensor nodes (say, 500 as in Figure 6(c)), even though $p^* \to 1$, the sensor nodes are never energy limited since they are scheduled less, energy obtained from ambient harvesting is enough.

The figures also include the IoT utilization calculated using the simple approximation in the previous section. Similar to the above discussion, the IoT network utilization first increases with p, since the spectrum availability limits the utilization, *i.e.*, $U_S^s \leq U_S^e$ in Equation (18). When the energy is the limiting factor, *i.e.*, $U_S^s > U_S^e$, the utilization decreases as p increases. As seen, the simple approximation overestimates the IoT utilization for given SN traffic patterns, however, it becomes more accurate as the number of sensor nodes increases. In the figures, we also observe that the SN traffic pattern plays an important role in the IoT utilization levels, especially when the number of sensor nodes in the network is small. In this case, an SN traffic with shorter bursts (larger β_s) provides a higher utilization level than a pattern with longer bursts since queue overflows occur less frequently.

A final note on Figure 6 is on the accuracy of the decoupling assumption. Although the Markov chain analysis follows the Monte Carlo results in all plots, the deviation is largest when there is only one SN. When number of SNs are 50 or 500, the difference is not significant. This observation coincides with the analysis of Section 4.1.

In the subsequent plots, for each data point, the optimal scheduling probability, p^* is calculated numerically and the corresponding utilization levels under such optimal energy transfer policies are reported.

In Figure 7, we investigate the cellular, IoT and sum utilization levels as a function of the number of sensor nodes. We observe that, as the number of nodes increases, the IoT network utilization increases. This increase is due to a multiuser gain, observed thanks to the broadcast nature

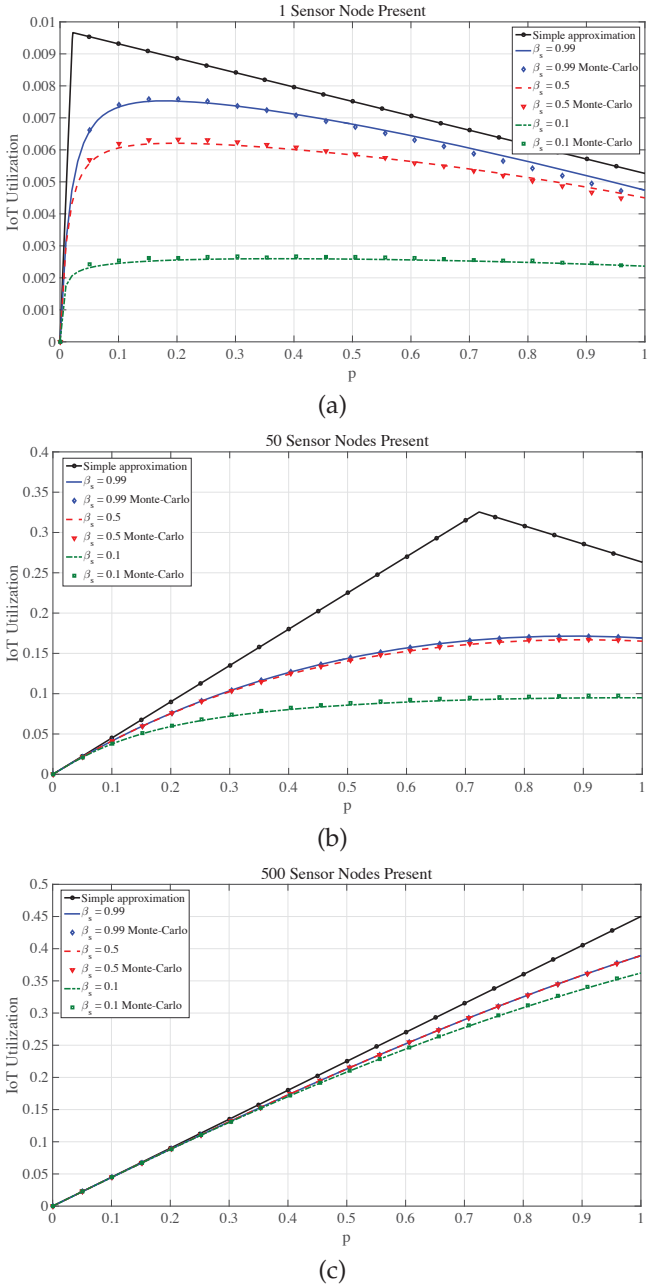

Fig. 6. IoT network utilization levels with respect to scheduling probability p, for $\beta_s \in \{0.1, 0.5, 0.99\}$. (a) $N_s = 1$, (b) $N_s = 50$ and (c) $N_s = 500$ sensor nodes are present. Note that $\beta_s = 0.99$ and $\beta_s = 0.5$ curves are too close to discern in (c). Other parameters are set to the defaults given in Table 2.

of energy transmission. In other words, as the number of nodes increases, more sensor nodes harvest the ambient or transferred energy. Even though the increase in the number of nodes inversely impacts the probability of scheduling for a given sensor node and lowers its individual utilization level, the total IoT network utilization increases. If the broadcast gain in the total harvested energy were absent, the IoT network utilization would have remained unchanged with respect to the number of sensor nodes.

The presence of the opportunistic IoT network is observed to have no impact on the cellular utilization, since the cellular utilization curve in the presence of opportunistic IoT

This article has been accepted for publication in a future issue of this journal, but has not been fully edited. Content may change prior to final publication. Citation information: DOI 10.1109/TMC.2017.2740378, IEEE Transactions on Mobile Computing

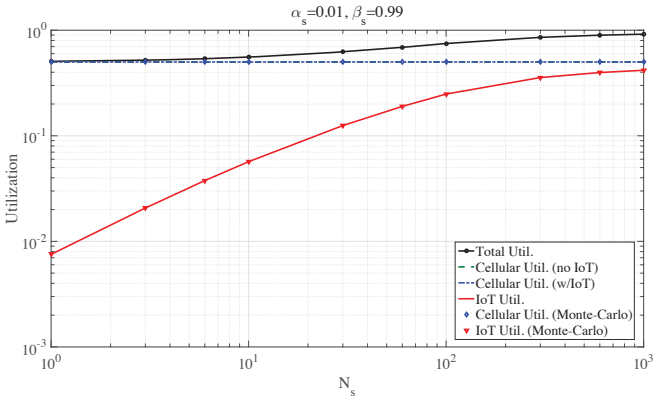

Fig. 7. The cellular, IoT and sum utilization levels with respect to number of sensor nodes present. Here, p is numerically optimized for each point. Other parameters are set to defaults given in Table 2. The blue diamonds and red triangles respectively denote the cellular and IoT utilization results of the Monte-Carlo simulations. The cellular utilization curve in the presence of opportunistic IoT network overlaps with the utilization curve without the IoT network presence.

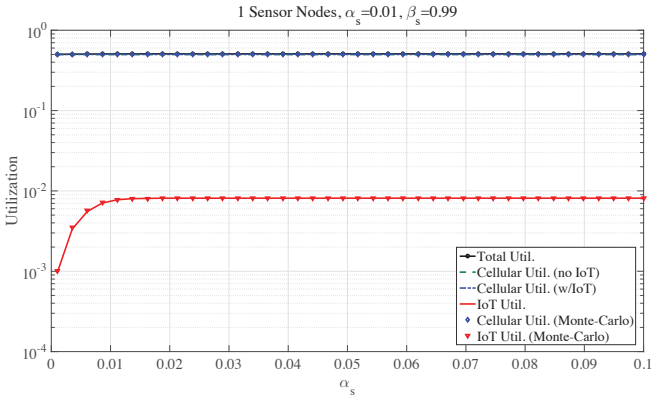

Fig. 8. The cellular, IoT and total utilization levels with respect to the SN traffic parameter α_s. Here, there is $N_s = 1$ SN present, $\beta = 0.5$, $\alpha = 0.5$, $\beta_s = 0.99$. p is numerically optimized for each point. Other parameters are set to defaults as given in Table 2. Note that the total utilization and both cellular utilization curves are too close to discern.

network overlaps with the utilization curve without the IoT network presence, thanks to the retransmissions employed by the cellular network. As shown in the results below, the effect of the IoT network presence on the cellular network utilization becomes more pronounced as the missed detection probability increases and maximum number of retransmissions decreases. The IoT network is shown to achieve a sum utilization level of more than 40% and a total cellular and IoT channel utilization of more than 90% for a network with as high as 500 sensor nodes without any impact on the cellular network utilization. This example demonstrates that this type of operation is suitable and feasible in green and spectrally efficient IoT networks, where there are many nodes with very low and bursty individual traffic loads.

Next, we consider an IoT network with a single SN, in order to investigate the effect of increasing SN traffic load demand on cellular and IoT utilization levels. This is illustrated in Figure 8. We observe that there is a maximum possible IoT utilization level for a given cellular traffic utilization and pattern (here, cellular load is 50% with $\alpha = \beta = 0.5$). As the SN traffic demand increases, p^* decreases to provide more energy for SN transmissions via energy transfer. However, beyond a certain point, the SN utilization level is bounded by the available spectrum, which is limited by the cellular traffic load and the minimum necessary spectrum for energy transfer by CLH to satisfy this utilization level. This example illustrates that, with RF energy harvesting and transfer, high individual traffic loads for SNs are infeasible; once again confirming that the system presented herein is most suitable for an IoT operation with very low and bursty individual traffic loads.

Next, we investigate the behavior of the cellular and IoT utilization levels as a function of increasing cellular traffic load. This is illustrated in Figure 9. Clearly, when the cellular traffic load increases, there is less spectrum available for the IoT network. When there is a single sensor node in the IoT network (Figure 9 (a)-(b)), the impact of the cellular traffic load increase on the IoT utilization is negligible, since the utilization of a single sensor node is

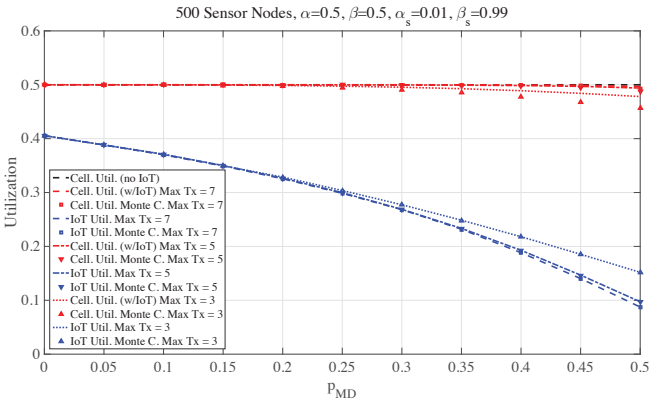

Fig. 10. The cellular and IoT utilization levels with respect to missed detection probability for varying maximum number of allowed cellular transmissions. Here, there are $N_s = 500$ SNs present, $\beta = 0.5$, $\alpha = 0.5$, $\beta_s = 0.99$. p is numerically optimized for each point. Other parameters are set to defaults as given in Table 2.

bounded by limited available energy and it is too small to be impacted by any increase in the cellular traffic load. For both Figures 9 (a) and (b), the traffic demand of the sensor node is $\alpha_s/(\alpha_s + \beta_s) = 1\%$, however, the actual α_s and β_s values in Figure 9 (a) represent a burstier traffic compared to Figure 9 (b). The conclusion is different, however, when there are many sensor nodes in the IoT network (Figure 9 (c)-(d)). We observe that increasing the cellular traffic load negatively impacts the sum IoT utilization level, since this increase lowers the available spectrum that sensor nodes could enjoy, due to the observed multiuser gain previously.

Last, we investigate the impact of sensing performance on the utilization levels. In Figure 10, we plot the cellular and IoT network utilization levels with respect to the probability of missed detection p_{MD}, for varying maximum number of allowed cellular transmissions N. Without loss of generality, p_{MD} is swept between 0 and 0.5, since any decision function that results in a $p_{\text{MD}} > 0.5$ can be flipped to achieve $p_{\text{MD}} \leq 0.5$. In the figure, the dashed black horizontal line at utilization=0.5 (visible toward the right of the figure) represents the cellular network utilization level when no IoT operation exists.

This article has been accepted for publication in a future issue of this journal, but has not been fully edited. Content may change prior to final publication. Citation information: DOI 10.1109/TMC.2017.2740378, IEEE Transactions on Mobile Computing

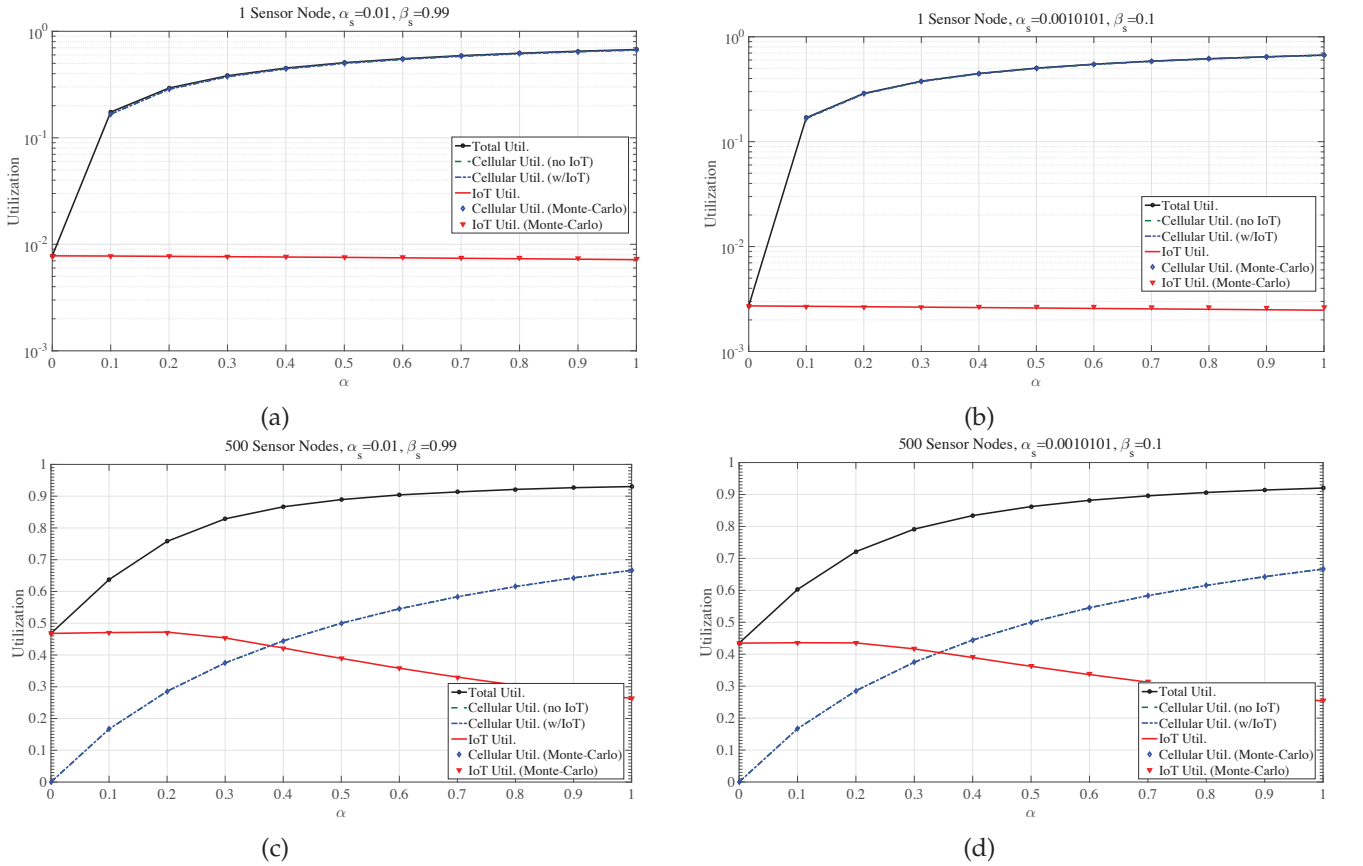

Fig. 9. The cellular, IoT and total utilization levels with respect to the cellular traffic parameter α for various N_s, α_s and β_s values. p is numerically optimized for each point. Other parameters are set to defaults as given in Table 2. The blue diamonds and red triangles respectively denote the cellular and IoT utilization results of the Monte-Carlo simulations. Note that both cellular utilization curves are too close to discern in all plots. They are also very close to total utilization curves in (a) and (b).

As mentioned earlier, for low p_{MD} and for high N, the impact of IoT operation on the cellular network is small even though the IoT network achieves about 40% utilization. Due to the retransmissions by the cellular network, most packets can be eventually transmitted. However as p_{MD} increases and N decreases, the impact of the IoT network on the cellular utilization is clearly visible. The IoT utilization also drops with larger p_{MD}, since collided packets are assumed to be lost for both networks. On the other hand for larger p_{MD}, IoT utilization increases with smaller N, as the IoT network finds more spectrum opportunities.

Another important observation is the increase in the deviation of cellular network utilization levels between the Markov Chain model's prediction and Monte-Carlo simulations as p_{MD} increases. This is in agreement with the discussion in Section 4.1; when the collision probability increases, the decoupling assumption starts to fail. However it is notable that even until p_{MD} is as high as 0.3, which is arguably too high for any practical opportunistic spectrum reuse scenario, the Markov Chain analysis and Monte-Carlo results are very close. Therefore, for our simulation setting, we conclude that the decoupling assumption is reasonable for practical systems.

7 Conclusion

We propose, for the first time, a cellular IoT network that performs RF energy harvesting and transfer, and shares its spectrum opportunistically with other cellular network services. The proposed slot-synchronous IoT network is composed of two types of nodes: a cluster head (CLH) with a reliable source of energy that conducts error-prone sensing of the cellular traffic and randomly schedules energy-harvesting sensor nodes (SNs) for information transfer. The CLH also randomly allocates some of its perceived idle channel time for energy transfer to SNs, which harvest energy either from the transmission of the cellular network or from the energy transfer of the CLH. In this framework, we demonstrate the interplay between the spectrum availability, energy availability, information and energy transfer operations using an inter-dependent Markov chain analysis and observe that there is a multi-user gain in the sum utilization due to the broadcast nature of the energy transmission; as the number of sensor nodes increases, IoT network utilization increases although individual utilizations decrease. We demonstrate that the proposed cellular IoT network is a feasible candidate for 5G, especially for a green, energy and spectrally efficient sensor network operation with high number of nodes demanding very low and bursty individual traffic loads.

References

[1] J. Gubbi, R. Buyya, S. Marusic, and M. Palaniswami, "Internet of Things (IoT): A vision, architectural elements, and future direc-

tions," *Future Gener. Comput. Syst.*, vol. 29, no. 7, pp. 1645–1660, Sep. 2013.

[2] S. Amendola, R. Lodato, S. Manzari, C. Occhiuzzi, and G. Marrocco, "RFID Technology for IoT-based Personal Healthcare in SmartSpaces," *IEEE Internet Things J.*, vol. 1, no. 2, pp. 144–152, 2014.

[3] N. Bui, A. P. Castellani, P. Casari, and M. Zorzi, "The internet of energy: A web-enabled smart grid system," *IEEE Netw.*, vol. 26, no. 4, pp. 39–45, 2012.

[4] L. Foschini, T. Taleb, A. Corradi, and D. Bottazzi, "M2M-based metropolitan platform for IMS-enabled road traffic management in IoT," *IEEE Commun. Mag.*, vol. 49, no. 11, pp. 50–57, 2011.

[5] A. Zanella, N. Bui, A. Castellani, L. Vangelista, and M. Zorzi, "Internet of Things for Smart Cities," *IEEE Internet Things J.*, vol. 1, no. 1, pp. 22–32, 2014.

[6] K. Fleming, P. Waweru, M. Wambua, E. Ondula, and L. Samuel, "Toward Quantified Small-Scale Farms in Africa," *IEEE Internet Comput.*, no. May/June, pp. 63–67, 2016.

[7] M. T. Lazarescu, "Design of a WSN platform for long-term environmental monitoring for IoT applications," *IEEE Trans. Emerg. Sel. Topics Circuits Syst.*, vol. 3, no. 1, pp. 45–54, 2013.

[8] H. S. Dhillon, H. Huang, and H. Viswanathan, "Wide-area Wireless Communication Challenges for the Internet of Things," *ArXiv e-prints*, Apr. 2015. [Online]. Available: https://arxiv.org/abs/1504.03242

[9] J. Gozalvez, "New 3GPP Standard for IoT [Mobile Radio]," *IEEE Veh. Technol. Mag.*, vol. 11, no. 1, pp. 14–20, March 2016.

[10] E. Borgia, "The internet of things vision: Key features, applications and open issues," *Comput. Commun.*, vol. 54, pp. 1–31, 2014.

[11] R. V. Prasad, S. Devasenapathy, V. S. Rao, and J. Vazifehdan, "Reincarnation in the Ambiance: Devices and networks with energy harvesting," *IEEE Commun. Surveys Tuts.*, vol. 16, no. 1, pp. 195–213, 2014.

[12] T. Rault, A. Bouabdallah, and Y. Challal, "Energy Efficiency in Wireless Sensor Networks: a top-down survey," *Comput. Netw.*, vol. 67, no. 4, pp. 104–122, 2014.

[13] S. Ulukus, A. Yener, E. Erkip, O. Simeone, M. Zorzi, P. Grover, and K. Huang, "Energy Harvesting Wireless Communications: A Review of Recent Advances," *IEEE J. Sel. Areas Commun.*, vol. 33, no. 3, pp. 360–381, 2015.

[14] S. Kitazawa, H. Ban, and K. Kobayashi, "Energy harvesting from ambient rf sources," in *Proc. of IEEE MTT-S*, May 2012, pp. 39–42.

[15] X. Lu, P. Wang, D. Niyato, D. I. Kim, and Z. Han, "Wireless networks with RF energy harvesting: A contemporary survey," *IEEE Commun. Surveys Tuts.*, vol. 17, no. 2, pp. 757–789, 2015.

[16] S. Lee, R. Zhang, and K. Huang, "Opportunistic wireless energy harvesting in cognitive radio networks," *IEEE Trans. Wireless Commun.*, vol. 12, no. 9, pp. 4788–4799, September 2013.

[17] A. Osseiran, J. F. Monserrat, and P. Marsch, Eds., *5G Mobile and Wireless Communications Technology*. Cambridge University Press, June 2016.

[18] Ericsson, "Ericsson Mobility Report on the Pulse of the Networked Society," Tech. Rep., November 2015. [Online]. Available: http://www.ericsson.com/res/docs/2015/mobility-report/ericsson-mobility-report-nov-2015.pdf

[19] E. Hossain and M. Hasan, "5G cellular: Key enabling technologies and research challenges," *IEEE Trans. Instrum. Meas.*, vol. 18, no. 3, pp. 11–21, 2015.

[20] P. Kamalinejad, C. Mahapatra, Z. Sheng, S. Mirabbasi, V. C. M. Leung, and Y. L. Guan, "Wireless Energy Harvesting for the Internet of Things," *IEEE Commun. Mag.*, no. 6, pp. 102–108, 2015.

[21] M. Garlatova, G. Grebla, M. Cong, I. Kymissis, and G. Zussman, "Movers and Shakers: Kinetic Energy Harvesting for the Internet of Things," *IEEE J. Sel. Areas Commun.*, no. 8, pp. 1624–1639, 2015.

[22] L. Liu, R. Zhang, and K.-C. Chua, "Wireless information transfer with opportunistic energy harvesting," *IEEE Trans. Wireless Commun.*, vol. 12, no. 1, pp. 288–300, January 2013.

[23] S. Luo, R. Zhang, and T. J. Lim, "Optimal save-then-transmit protocol for energy harvesting wireless transmitters," *IEEE Trans. Wireless Commun.*, vol. 12, no. 3, pp. 1196–1207, March 2013.

[24] S. Yin, E. Zhang, L. Yin, and S. Li, "Optimal saving-sensing-transmitting structure in self-powered cognitive radio systems with wireless energy harvesting," in *Proc. of IEEE ICC*, June 2013, pp. 2807–2811.

[25] R. Zhang and C. K. Ho, "Mimo broadcasting for simultaneous wireless information and power transfer," *IEEE Trans. Wireless Commun.*, vol. 12, no. 5, pp. 1989–2001, May 2013.

[26] G. Zheng, Z. Ho, E. A. Jorswieck, and B. Ottersten, "Information and energy cooperation in cognitive radio networks," *IEEE Trans. Signal Process.*, vol. 62, no. 9, pp. 2290–2303, May 2014.

[27] M.-L. Ku, Y. Chen, and K. J. R. Liu, "Data-Driven Stochastic Models and Policies for Energy Harvesting Sensor Communications," *IEEE J. Sel. Areas Commun.*, vol. 33, no. 8, pp. 1505–1520, 2015.

[28] W. H. R. Chan, P. Zhang, I. Nevat, S. G. Nagarajan, A. C. Valera, H.-X. Tan, and N. Gautam, "Adaptive Duty Cycling in Sensor Networks With Energy Harvesting Using Continuous-Time Markov Chain and Fluid Models," *IEEE J. Sel. Areas Commun.*, vol. 33, no. 12, pp. 2687–2700, 2015.

[29] D. T. Hoang, D. Niyato, P. Wang, D. I. Kim, and S. Member, "Opportunistic Channel Access and RF Energy Harvesting in Cognitive Radio Networks," *IEEE J. Sel. Areas Commun.*, vol. 32, no. 11, pp. 2039–2052, 2014.

[30] D. T. Hoang, D. Niyato, P. Wang, and D. I. Kim, "Performance Optimization for Cooperative Multiuser Cognitive Radio Networks with RF Energy Harvesting Capability," *IEEE Trans. Wireless Commun.*, vol. 14, no. 7, pp. 3614–3629, 2015.

[31] S. Yin, Z. Qu, and S. Li, "Achievable Throughput Optimization in Energy Harvesting Cognitive Radio Systems," *IEEE J. Sel. Areas Commun.*, vol. 33, no. 3, pp. 407–422, 2015.

[32] J. Kim and G. Hwang, "Stability Analysis of Multi-Channel Cognitive Radio Networks Based on Decoupling Approach," in *Proc. of Ubiquitous and Future Netw.*, 2015, pp. 645–650.

[33] N. Tadayon and S. Aïssa, "Multi-Channel Cognitive Radio Networks: Modeling, Analysis and Synthesis," *IEEE J. Sel. Areas Commun.*, vol. 32, no. 11, pp. 2065–2074, 2014.

[34] N. Tadayon and S. Aïssa, "Modeling and Analysis Framework for Multi-Interface Multi-Channel Cognitive Radio Networks," *IEEE Trans. Wireless Commun.*, vol. 14, no. 2, pp. 935–947, 2015.

[35] T. Yucek and H. Arslan, "A survey of spectrum sensing algorithms for cognitive radio applications," *IEEE Commun. Surveys Tuts.*, vol. 11, no. 1, pp. 116–130, 2009.

[36] M. Sahin, I. Guvenc, M. R. Jeong, and H. Arslan, "Handling CCI and ICI in OFDMA femtocell networks through frequency scheduling," *IEEE Trans. Consum. Electron.*, vol. 55, no. 4, pp. 1936–1944, 2009.

[37] S. Geirhofer and L. Tong, "Dynamic Spectrum Access in the Time Domain : Modeling and Exploiting White Space," *IEEE Commun. Mag.*, no. May, pp. 66–72, 2007.

[38] M. Levorato, U. Mitra, and M. Zorzi, "Cognitive interference management in retransmission-based wireless networks," *IEEE Trans. Inf. Theory*, vol. 58, pp. 3023–3046, May 2012.

[39] M. Levorato, S. Firouzabadi, and A. Goldsmith, "A learning framework for cognitive interference networks with partial and noisy observations," *IEEE Trans. Wireless Commun.*, vol. 11, pp. 3101–3111, September 2012.

[40] G. Bianchi, "Performance analysis of the IEEE 802.11 distributed coordination function," *IEEE J. Sel. Areas Commun.*, vol. 18, pp. 535–547, March 2000.

[41] A. Kumar, E. Altman, D. Miorandi, and M. Goyal, "New Insights From a Fixed-Point Analysis of Single Cell IEEE 802.11 WLANs," *IEEE/ACM Trans. Netw.*, vol. 15, no. 3, pp. 588–601, June 2007.

[42] V. Ramaiyan, A. Kumar, and E. Altman, "Fixed point analysis of single cell IEEE 802.11e WLANs: uniqueness, multistability and throughput differentiation," in *ACM SIGMETRICS Perform. Eval. Rev.*, vol. 33, no. 1. ACM, 2005, pp. 109–120.

[43] G. Sharma, A. Ganesh, and P. Key, "Performance analysis of contention based medium access control protocols," *IEEE Trans. Inf. Theory*, vol. 55, no. 4, pp. 1665–1682, 2009.

[44] J.-w. Cho, J.-Y. Le Boudec, and Y. Jiang, "On the asymptotic validity of the decoupling assumption for analyzing 802.11 MAC protocol," *IEEE Trans. Inf. Theory*, vol. 58, no. 11, pp. 6879–6893, 2012.

[45] A. Leon-Garcia, *Probability, Statistics, & Random Processes for Electrical Engineering*, 3rd ed. Prentice Hall, 2007.